JOURNAL OF BACTERIOLOGY, Nov. 1992, p. 6717–6728
0021-9193/92/216717-12$02.00/0

Vol. 174, No. 21

Identification of *Bacillus subtilis* Genes for Septum Placement and Shape Determination

PETRA ANNE LEVIN,[1] PETER S. MARGOLIS,[1] PETER SETLOW,[2]
RICHARD LOSICK,[1]* AND DONGXU SUN[2]

Department of Cellular and Developmental Biology, The Biological Laboratories, Harvard University, Cambridge, Massachusetts 02138,[1] and Department of Biochemistry, University of Connecticut Health Center, Farmington, Connecticut 06032[2]

Received 29 May 1992/Accepted 17 August 1992

The *Bacillus subtilis divIVB1* mutation causes aberrant positioning of the septum during cell division, resulting in the formation of small, anucleate cells known as minicells. We report the cloning of the wild-type allele of *divIVB1* and show that the mutation lies within a stretch of DNA containing two open reading frames whose predicted products are in part homologous to the products of the *Escherichia coli* minicell genes *minC* and *minD*. Just upstream of *minC* and *minD*, and in the same orientation, are three genes whose products are homologous to the products of the *E. coli* shape-determining genes *mreB*, *mreC*, and *mreD*. The *B. subtilis* *mreB*, *mreC*, and *mreD* genes are the site of a conditional mutation (*rodB1*) that causes the production of aberrantly shaped cells under restrictive conditions. Northern (RNA) hybridization experiments and disruption experiments based on the use of integrational plasmids indicate that the *mre* and *min* genes constitute a five-cistron operon. The possible involvement of *min* gene products in the switch from medial to polar placement of the septum during sporulation is discussed.

Cells of the gram-positive soil bacterium *Bacillus subtilis* are capable of entering an alternative developmental pathway that is characterized by the formation of a transverse septum. During vegetative growth, the formation of a septum at the center of the cell partitions the bacterium into identical daughter cells which separate and undergo further cycles of binary fission. The hallmark of the process of sporulation, in contrast, is the formation of a septum that is sited near one pole of the cell. This asymmetrically positioned septum partitions the bacterium into unequal-sized cellular compartments, of which one, the forespore, undergoes metamorphosis into a spore and the other, the mother cell, participates in the formation of the spore but is eventually discarded by lysis. The binary fission septum and the sporulation septum are produced by similar processes (17), involving in both cases the action of *B. subtilis* homologs to the *Escherichia coli* septation genes *ftsA* and *ftsZ* (2, 3). However, little is known about the mechanisms that govern the alternative placement of the septa at medial or polar positions within the cell.

In the non-spore-forming bacterium *E. coli*, placement of the septum is governed by genes at the *minB* locus. Cells of *E. coli* grow by binary fission and are normally capable of producing only medially sited septa. However, certain mutations at the *minB* locus allow septa to form at a polar position, thereby generating small, anucleate cells with intact cell walls and membranes which except for their lack of DNA appear to be metabolically normal (1). Minicell production occurs as an alternative to normal division, and consequently, the sister cell is filamentous and carries two or more copies of the chromosome. Because the minicell division process appears to be identical to that of the wild type, the defect is apparently with site selection and not with septum formation. As with sporulation in *B. subtilis*, minicell formation in *E. coli* involves the asymmetric positioning of the septum. Unlike sporulating *B. subtilis* cells, minicell mutants are defective in nucleoid segregation, so minicells are devoid of a chromosome.

The *minB* locus is an operon consisting of genes *minC*, *minD*, and *minE* (8, 10, 11). Under normal conditions, the gene products of *minC* and *minD* act in concert to form an inhibitor of cell division at the three potential division sites: midcell and the two poles. The MinCD complex is given its topological specificity by a third protein, MinE, which blocks the activity of the division inhibitor at midcell, thereby ensuring that the division septum is correctly positioned. Placement of septa at polar locations, the minicell phenotype, occurs in the absence of the *minC* and *minD* gene product or as a result of the overexpression of the *minE* gene. In contrast, as a consequence of the overexpression of *minCD* or a null mutation in *minE*, cells are filamentous in appearance. Deletion of the entire *minB* locus results in a minicell phenotype, indicating that the genes are not required for growth. It appears that placement of the septum in minicell mutants is a nonrandom process which relies on the existence of division sites, the positions of which are strictly determined in *minB* mutants as well as in wild-type cells prior to the beginning of septation (19). The *minC* gene product has been implicated in a second-division pathway involving the gene *dicB* (12, 21), and MinCD is also known to interact with FtsZ to antagonize its cell division activity (4). For a review of the models that explain the regulation of cell division, see de Boer et al. (9).

Is the placement of the sporulation septum in *B. subtilis* governed by genes similar to those of the *minB* operon? In a manner similar to septation in minicell mutants, septum formation in vegetative or sporulating *B. subtilis* cells always occurs at the same positions, either at midcell or in a polar location, indicating that septum placement is not a random process and that certain potential division sites must exist prior to septation. It may be that sporulating *B. subtilis* cells take advantage of the polar division sites to position the asymmetric septum, as pointed out by Beall and Lutkenhaus

* Corresponding author.

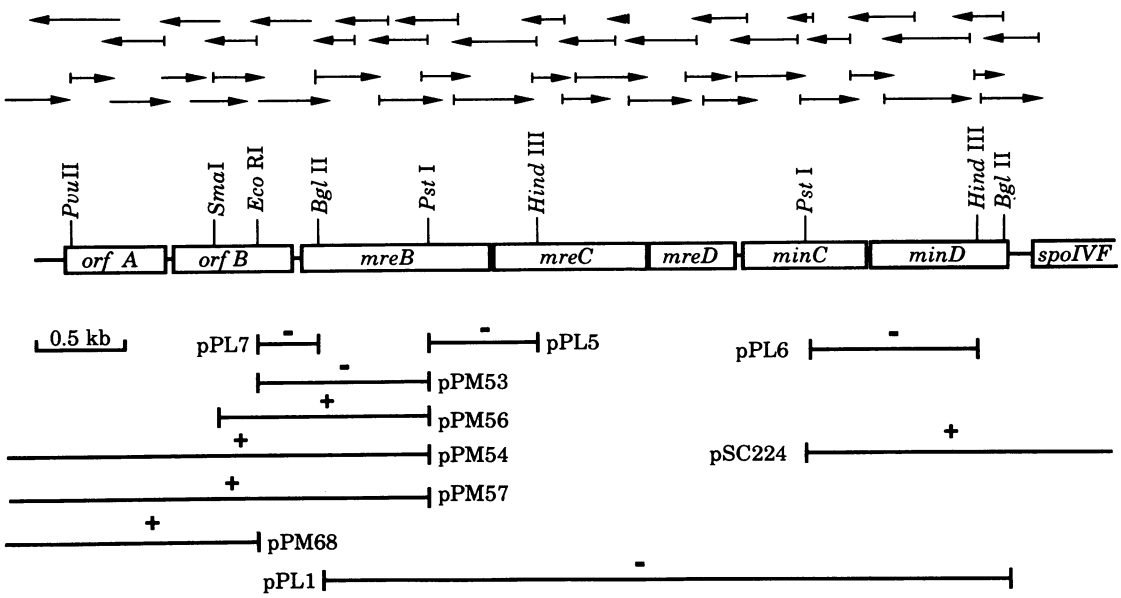

FIG. 1. Physical and restriction maps of the *divIVB* region of the chromosome. Arrows at the top indicate the sequencing strategy used to determine the nucleotide sequences of the two upstream ORFs and those of the five ORFs within the *mreBCD* and *minCD* operon. Bases of the arrows denote whether the sequence was obtained from a restriction endpoint (small bar) or a synthetic oligonucleotide (no symbol). Each rectangle represents an ORF, all of which are transcribed from left to right. The lower part of the figure shows the plasmid inserts which were used to determine the boundaries of the *divIVB* operon. The inserts in plasmids pPM56, pPM54, pPM57, pPM68, and pSC224 extend beyond the boundaries of this diagram. Symbols above each insert indicate whether integration of the plasmid into wild-type strain PY79 resulted in a wild-type (+) or a minicell (−) phenotype.

(2). Thus, the gene products from a developmentally regulated *minB*-like locus are candidates for the accurate positioning of the septum during sporulation and vegetative growth in *B. subtilis*.

As a first step towards characterizing the cellular mechanisms that govern septum placement in *B. subtilis*, we attempted to isolate and characterize the *divIVB* locus, at which a mutation causes the production of small, anucleate minicells (29). Because of the phenotypic similarity between the *E. coli min* mutants and the *B. subtilis divIVB1* mutant, we anticipated that the *divIVB* locus might be the *B. subtilis* homolog to the *minB* locus of *E. coli*.

We report here that the *divIVB1* mutation lies within an operon that contains homologs to the *E. coli minC* and *minD* genes but not the the *E. coli minE* gene. Immediately upstream of and cotranscribed with *minC* and *minD* are three genes whose products are homologs of the *E. coli* shape-determining genes *mreB*, *mreC*, and *mreD*. The *mre* genes are the site of the previously identified *rodB1* mutation, which causes the production of aberrantly shaped cells under restrictive conditions (32). We discuss the possible role for *B. subtilis minC* and *minD* in the regulation of asymmetric septation during sporulation.

MATERIALS AND METHODS

Bacterial strains. The wild-type strain used in this study was PY79, the prototrophic derivative of PY78 (43). Strains 1A292 (*divIVB1 metB5 thyA1 thyB1*) (29) and 1A485 (*rodB1 leuA8*) (32) were obtained from the *Bacillus* Genetics Stock Center (The Ohio State University). The construction of PL9, a *divIVB1* mutant strain congenic with PY79, is described below.

General methods. Competent cells were prepared and transformed as described by Dubnau and Davidoff-Abelson (14). Selection for Cm^r was conducted on Luria-Bertani (LB) agar containing 5 μg of chloramphenicol per ml.

Sporulation was induced in liquid in Difco sporulation (DS) medium and on plates with DS agar (28).

DNA manipulations in *E. coli* were carried out as described by Sambrook et al. (33).

Microscopic analysis of mutant strains was performed by using phase-contrast optics on a Zeiss microscope at ×1,000 magnification. Cells were photographed with bright-field optics at the same magnification.

Construction of strain PL9. Because of a competence defect in the *divIVB1* mutant strain (1A292) we obtained from the *Bacillus* Genetics Stock Center, it was necessary to move *divIVB1* into a competence-proficient background. To construct this new strain, we transformed chromosomal DNA from 1A292 into the Spo^- strain SC834 (*spoIVFB152*) (6), a strain which is congenic to PY79. We chose strain SC834 because of the close proximity between the *spoIVF* locus and the *divIVB* locus. The scheme was to use the 1A292 chromosome to correct the sporulation mutation and select for cells which were Spo^+; Spo^+ transformants were then screened for those which were mutant at the *divIVB* locus but did not exhibit the original competence defect.

Spo^+ transformants were selected via chloroform resistance (7, 18), and resulting Spo^+ colonies were screened for minicell production and competence. One such Spo^+ Min^- Com^+ transformant was designated PL9.

Plasmids. Plasmid pSC224 (6) has an insert which extends from a restriction site internal to the *spoIVF* operon to a *Pst*I site upstream of the *spoIVFA* start codon (Fig. 1).

Plasmid pSR3 (31) was constructed by the method of Youngman (42) for cloning *B. subtilis* DNA adjacent to a transposon insertion. The insert in pSR3 extends from an *Eco*RI site within the Tn*917* transposon insertion in KS179

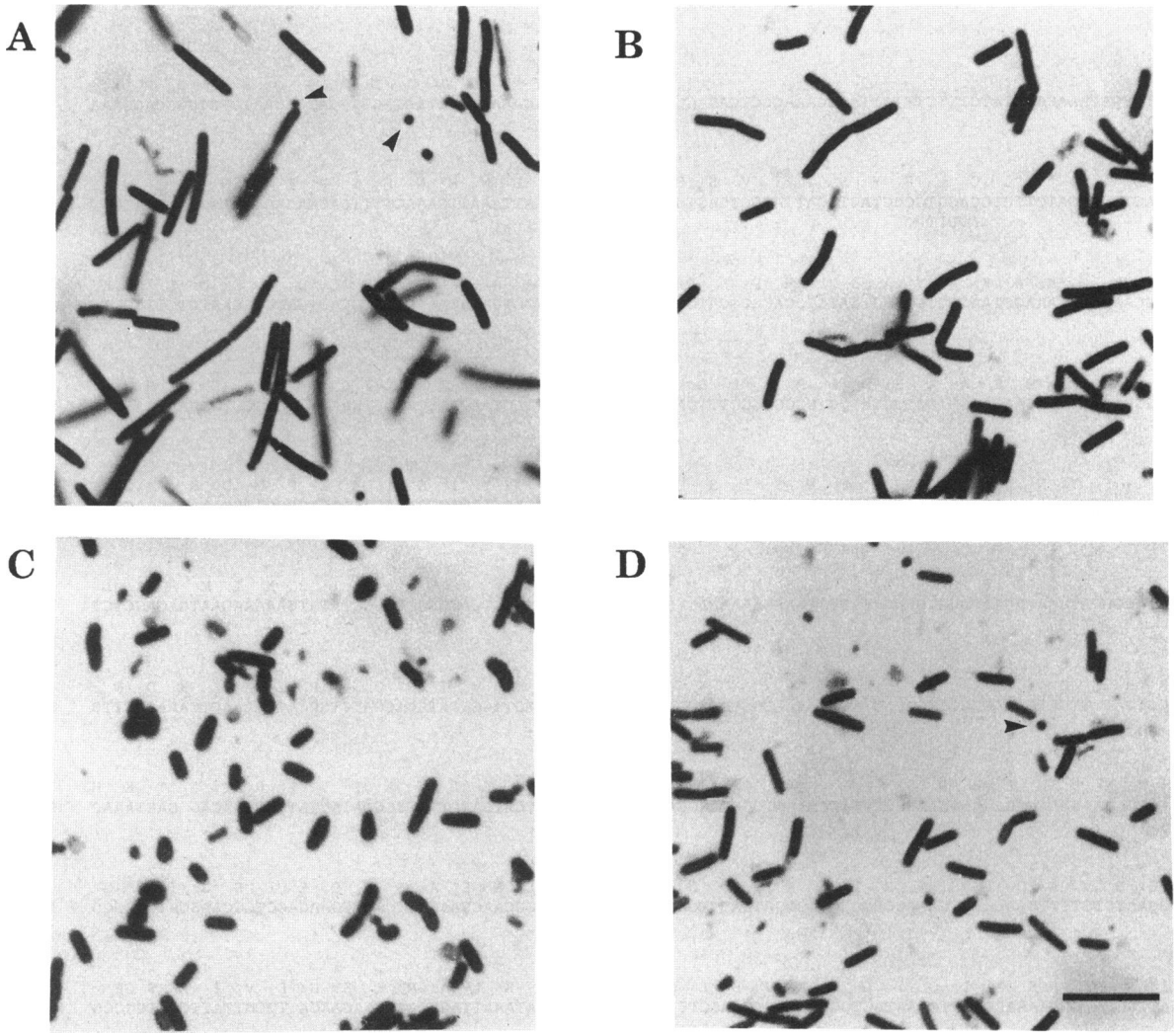

FIG. 2. Bright-field micrographs of *B. subtilis divIVB1* and *rodB1* mutants, showing corrected and uncorrected phenotypes. All cells were grown overnight on LB agar. Strain 1A485 cells and transformants were grown under nonpermissive conditions at 45°C. (A) Cells from strain PL9, which carries the original *divIVB1* mutation. Arrowheads indicate free and attached minicells. (B) Strain PL9 transformed with the integrational plasmid pSC224. Minicell phenotype is corrected. (C) Strain 1A485 exhibiting the classical *rodB1* mutation. (D) Strain 1A485 transformed with plasmid pPL1. Although the rod phenotype is corrected, integration of pPL1 results in a slight minicell defect. Arrowhead indicates free minicell. Magnification, ×6,000. Bar = 2 μm.

(34) (*spoIVFA*::Tn*917*ΩHU179) to the *Eco*RI site 4.3 kb upstream of the *spoIVFA* start codon (Fig. 1).

Plasmids pPL1, pPL5, and pPL6 (Fig. 1) were constructed by subcloning DNA from pSR3 into the integrational vector pSGMU2 (15). Plasmid pSGMU2 is a pUC13 derivative which contains the *bla* and *cat* genes and an origin of replication for *E. coli* but lacks an origin of replication for *B. subtilis*. Plasmid pPL1 was constructed by gel purifying a 3.7-kb *Bgl*II fragment from pSR3 by using the GeneClean Kit (Bio 101) and ligating the fragment into the *Bam*HI site in the polylinker of pSGMU2. Plasmids pPL5 and pPL6 were constructed in a similar manner from separate *Hin*dIII-*Pst*I fragments (0.9 and 1.1 kb, respectively) of pSR3.

Plasmids pPM53, pPM54, pPM56, pPM57, and pPM68 were constructed in other work (23) as part of an effort to clone *spoIIB*, which is located just upstream of *orfA*, by a chromosome-walking procedure. Plasmid pPL7 was constructed by subcloning the *Eco*RI-*Bgl*II fragment of pPM53 into the polylinker of pSGMU2 in the manner described above.

Correction of the *divIVB1* and *rodB1* mutations. To test the capacities of the plasmids described above to correct the *divIVB1* and *rodB1* mutations, competent cells from strains PL9 and 1A485 were transformed with the integrational plasmids, and transformants were selected by chloramphenicol resistance. Single crossover events between a wild-type plasmid insert and mutant chromosomal DNA can occur upstream or downstream of the mutation; those which occur upstream of the mutant allele will result in the correction of the mutation by the creation of a full-length wild-type copy of the gene.

We screened transformants of PL9 for correction of the *divIVB1* mutation and 1A485 for correction of the *rodB1* mutation by using phase-contrast microscopy. In the case of 1A485, transformants were examined following growth at the nonpermissive temperature of 45°C.

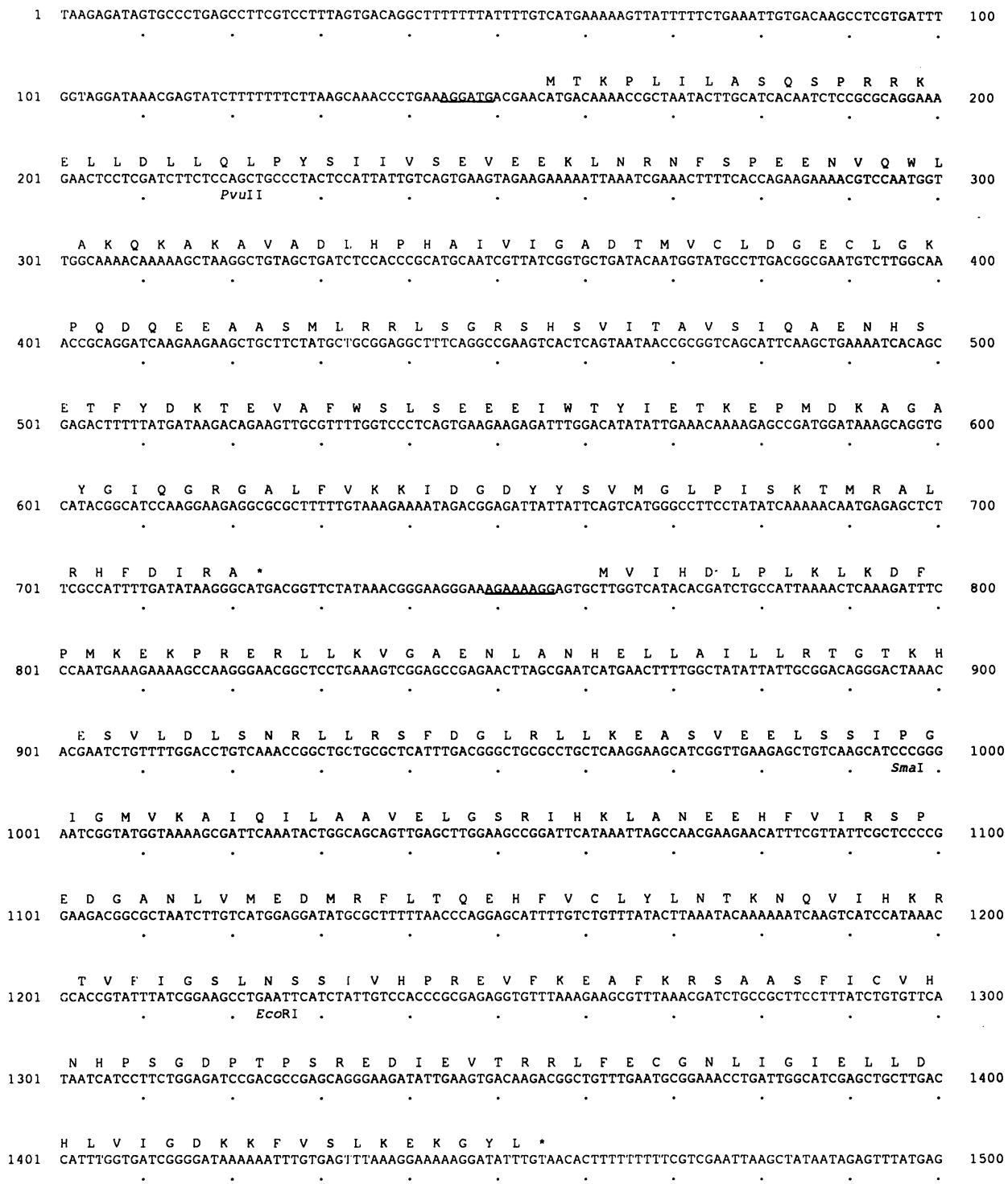

FIG. 3. Nucleotide sequence of the chromosomal region between *spoIIB* and *spoIVF* including amino acid sequences of the two upstream ORFs and of the five ORFs within the *mreBCD* and *minCD* operon. Restriction sites used for subcloning are indicated. Prospective ribosome-binding sites are underlined, and a potential rho-independent terminator is indicated by arrows. A nucleotide-binding site consensus sequence within the N terminus of *minD* is indicated by a line beneath the amino acid sequence. Asterisks denote stop codons.

Nucleotide sequencing. Nucleotide sequencing was carried out according to the method described by Sanger et al. (35) with the Sequenase kit (USB) with modifications for double-stranded sequencing. The strategy used is outlined schematically at the top of Fig. 1.

Heat killing procedure. To check PL9 for sporulation efficiency, we employed a modification of the assay for heat resistance outlined by Nicholson and Setlow (28). Following 2 days of growth in DS medium, cultures of PY79 and PL9 were serially diluted into 1× T base (7) and plated both prior

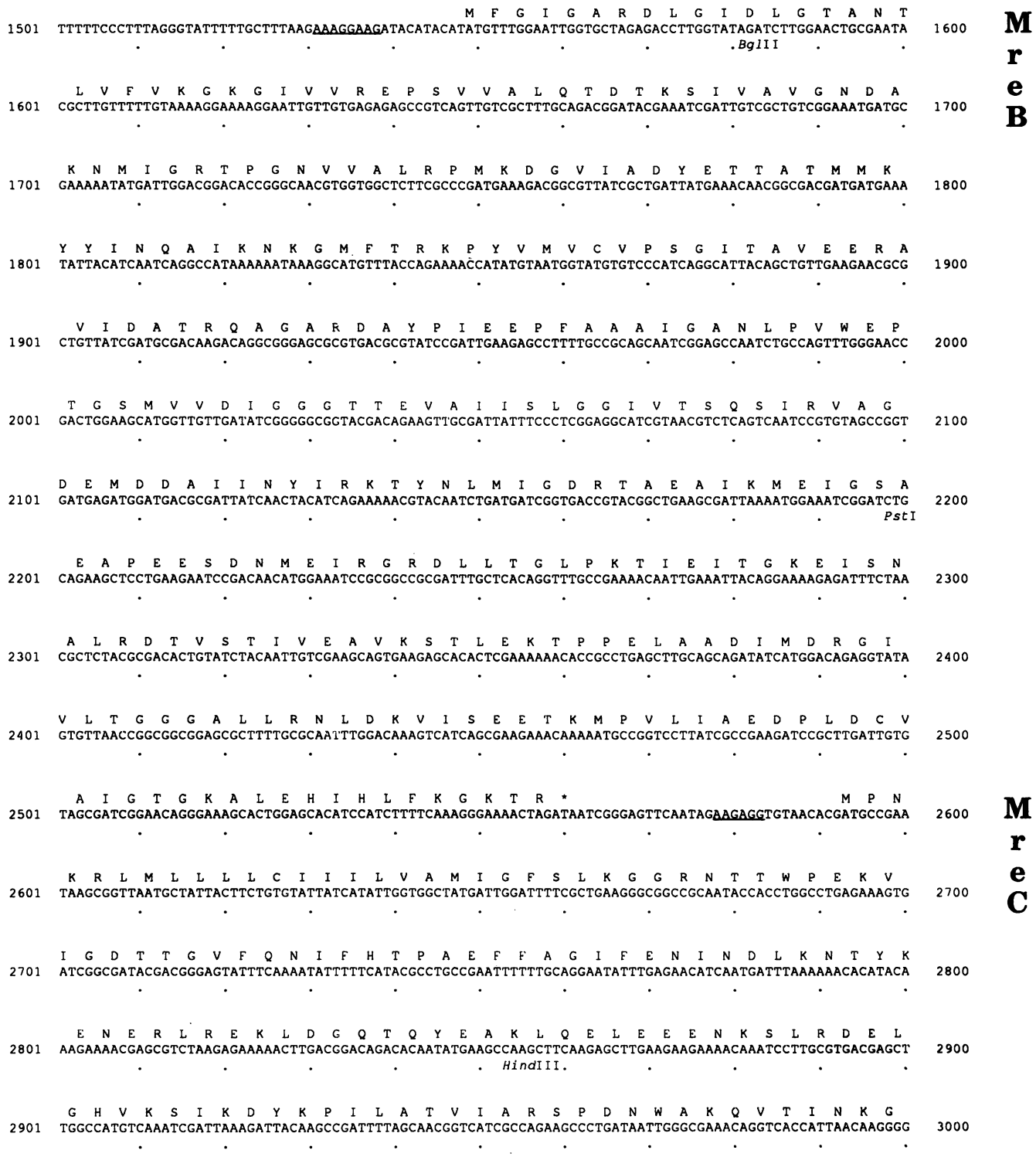

FIG. 3—*Continued.*

to and after a 15-min incubation at 80°C to determine the proportion of heat-resistant spores as a function of viable cell count.

Isolation of RNA. RNA for Northern (RNA) hybridization analysis was prepared from sporulating cells harvested just after and 2 h after the end of exponential growth in DS medium. The method of RNA isolation was as described by Roels et al. (30) except that we employed a slightly different resuspension buffer (100 mM LiCl, 10 mM EDTA, 10 mM Tris [pH 7.8], 1% sodium dodecyl sulfate) and the precipitated RNA was treated with DNase as a final step in the purification process.

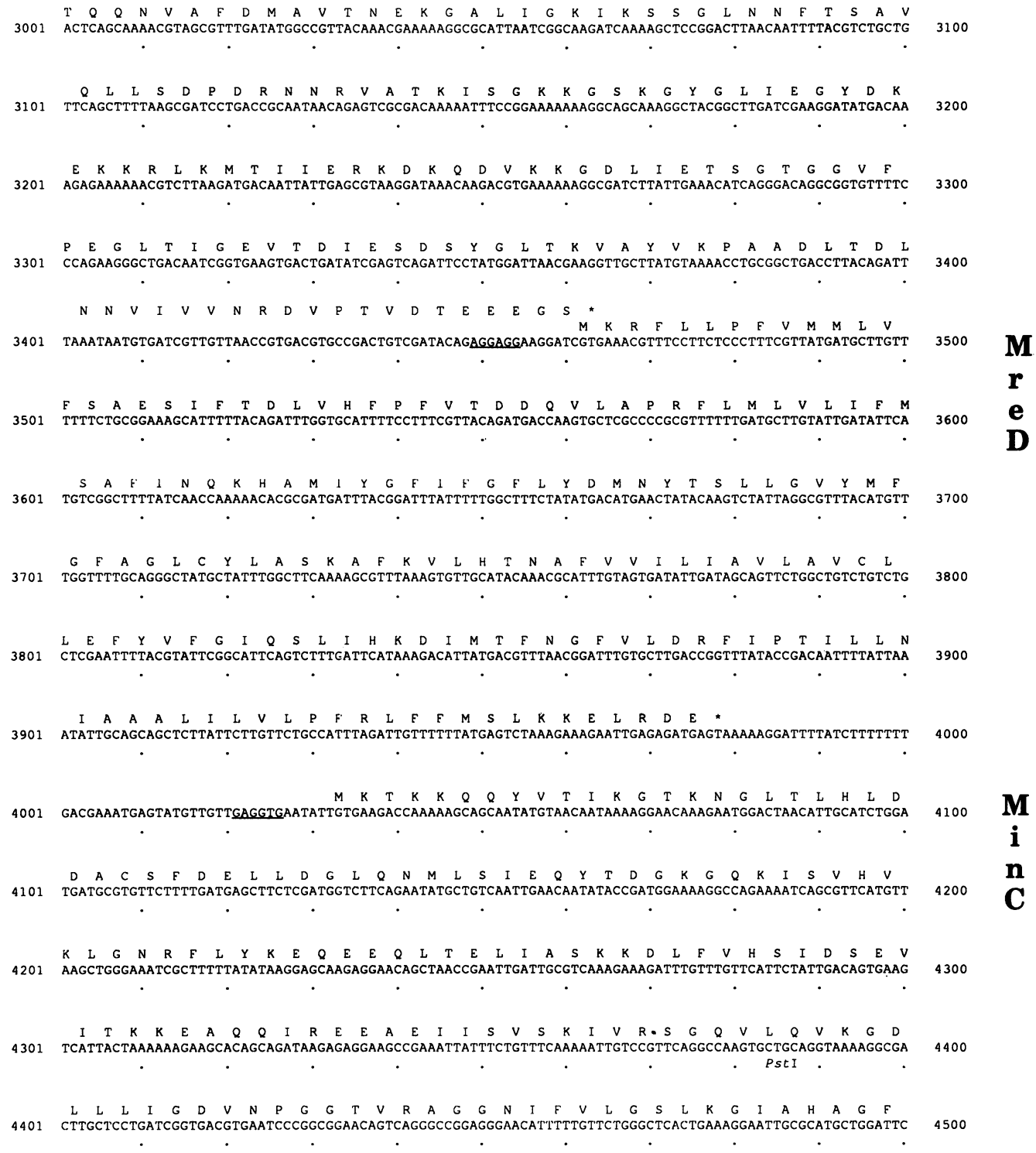

FIG. 3—*Continued.*

Northern hybridization analysis. Northern hybridization was carried out as a modification of the method presented in Sambrook et al. (33). Samples of RNA (10 and 30 μg) were loaded onto a 1.5% agarose gel containing 2.2 M formaldehyde. Following electrophoresis, the RNA was transferred to a nylon membrane (Hybond-N; Amersham). Prehybridization and hybridization were carried out at 65°C in hybridization buffer {50 mM PIPES [piperazine-*N*-*N*′-bis(2-ethanesulfonic acid)] pH 7.0], 50 mM Na_2PO_4 [pH 7.0], 100 mM NaCl, 10 mM EDTA, 5% sodium dodecyl sulfate}. The nick-translated inserts from pPL5 and pPL6 (Fig. 1) and an *Eco*RI fragment from pPM3 (23), which contains the

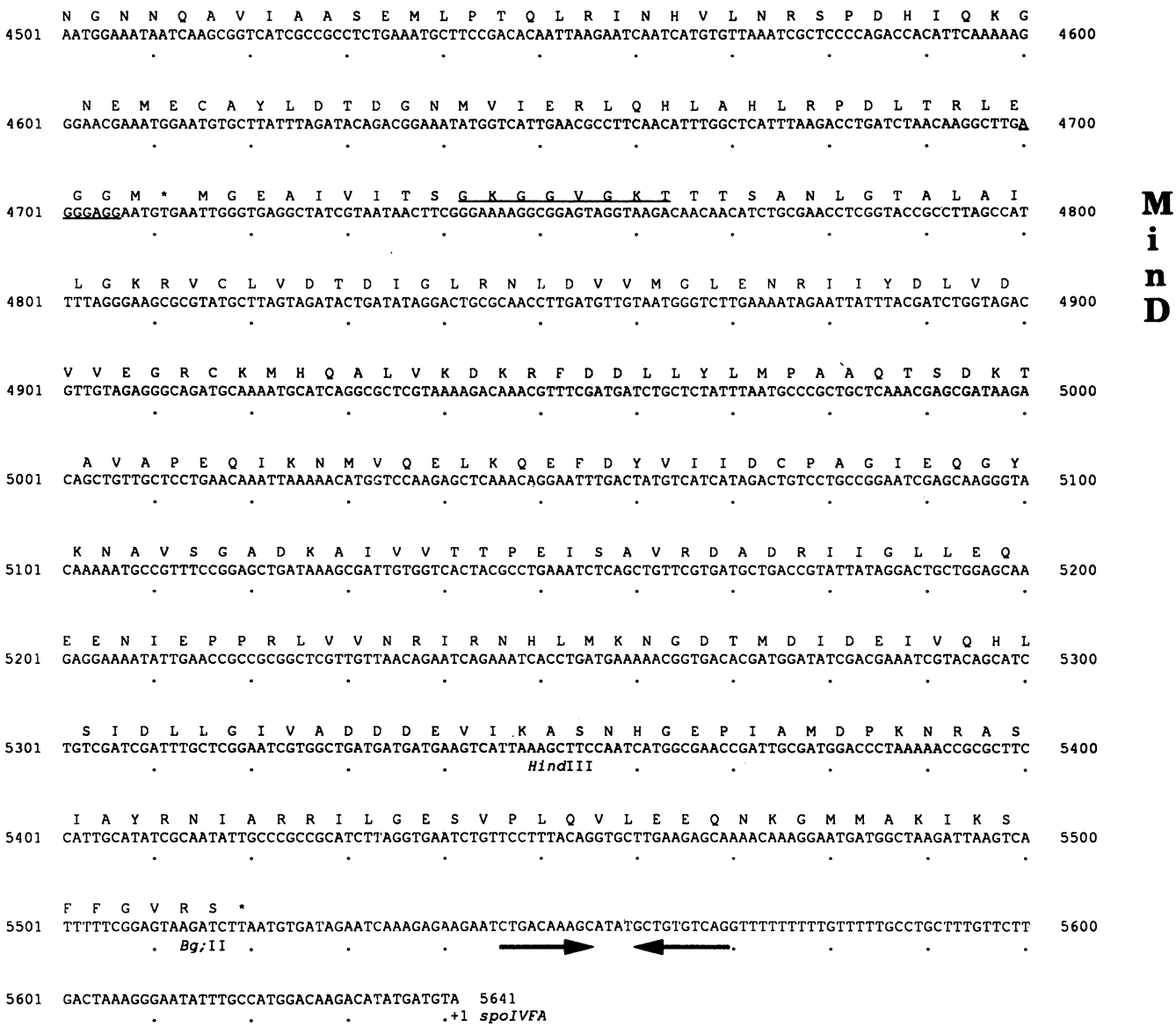

FIG. 3—*Continued.*

spoIIAC gene, were used as probes. A 0.24- to 9.5-kb RNA ladder (BRL) was used for molecular weight standards.

Staining procedure for light microscopy. We employed a modification of the staining procedure described by Miyakawa and Komano (24) to stain *Bacillus* mutants for light microscopy. Cells were grown overnight on LB agar. The *rodB1* strains were grown at the nonpermissive temperature of 45°C, while the *divIVB1* strains were grown at 37°C. Single colonies were picked from the plates and suspended in a mixture of 50 μl of LB and 50 μl of a 3% formaldehyde solution (3% formaldehyde in 50 mM sodium phosphate buffer [pH 7.0]). Cell suspensions were then smeared on glass microscope slides, flamed to fix the cells, and rinsed under running water for 3 min. The samples were then treated with drops of a 5% tannic acid solution (5% tannic acid in 50 mM sodium phosphate buffer [pH 7.0]) as a mordant, incubated on a heat block at 65°C for 2 min, and rinsed under running water for 3 additional minutes. A drop of crystal violet solution (0.02% crystal violet in 50 mM sodium phosphate buffer [pH 7.0]) was added to the sample, a coverslip was placed on top, and the cells were examined and photographed under bright-field optics at ×1,000 magnification.

Nucleotide sequence accession number. The sequences of the *divIVB* operon and two upstream open reading frames (ORFs) have been deposited in the GenBank data base under accession number M96343.

RESULTS

Localization and cloning of the *divIVB1* mutation. Previous mapping experiments have shown that the *divIVB1* mutation is located at about 247° on the genetic map of Henner and Hoch (16), the order of loci being *leuA*, *spoIIB*, *rodB*, *divIVB*, and *spoIVF* (22, 29). The availability of cloned *spoIVF* DNA (6) made it possible for us in other work (23) to

clone DNA extending from *spoIVF* to *spoIIB* via a chromosome-walking procedure. Figure 1 is a physical map of this segment of the chromosome, which was expected to contain the wild-type allele of *divIVB1*. The same chromosomal region of DNA was also cloned by an independent strategy based on the use of a library of random insertions in the *B. subtilis* chromosome of the integration vector pJH101. One such integrant, identified as exhibiting linkage to *divIVB1* by DNA-mediated transformation, was used to walk to the *divIVB* locus.

To localize *divIVB1*, we used integrational plasmids and various segments of cloned DNA from the region between *spoIVF* and *spoIIB* to correct the *divIVB1* mutation of the minicell-producing strain PL9, which is congenic to the *divIVB*$^+$ strain PY79. Integration into the chromosome of PL9 of pSC224 (6), whose insert extends from the downstream end of the *spoIVF* operon to a *Pst*I site that is approximately 1.3 kb upstream of the *spoIVFA* start codon (Fig. 1), was found to correct the *divIVB1* mutation (Fig. 2A and B). Similarly, integration of pPL1, whose insert extends from the *Bgl*II site just upstream of *spoIVF* to a second *Bgl*II site located approximately 4 kb further upstream, also corrected the *divIVB1* mutation, although the minicell phenotype of the resulting transformants was not fully wild type. (The reason that integration of pPL1 only partially suppressed the *divIVB1* phenotype is discussed below.) In contrast, the integration of pPM53 and pPM57 did not correct the mutation (Fig. 1). We conclude that the wild-type allele of the *divIVB1* mutation is located between the upstream boundary of the insert in pSC224 and the downstream boundary of the insert in pPL1, that is, between the *Pst*I and *Bgl*II sites indicated in Fig. 1.

Nucleotide sequencing of the *divIVB* region of the chromosome. Figure 3 shows the nucleotide sequence of DNA in the region from *spoIIB* to *spoIVF*. Sequencing was accomplished according to the strategy outlined in Materials and Methods and as indicated by the arrows at the top of Fig. 1. Starting from the left side of Fig. 1, nucleotide sequencing revealed the existence of seven major ORFs, all in a left-to-right orientation and all with preceding sequences that could serve as ribosome-binding sites according to Moran et al. (25). The first ORF (*orfA*) is expected to encode a 21-kDa polypeptide that is 189 amino acids in length. A GenBank search indicates that this polypeptide is approximately 70% similar at the amino acid level to an ORF (*orfE*) located immediately downstream of *E. coli mreD* (40), an observation to which we were alerted by G. Stewart (37). Intriguingly, *orfA* is located less than 1 kb upstream of an operon that includes the *B. subtilis* homologs to *E. coli mreB*, *mreC*, and *mreD* (see below).

The second ORF (*orfB*) encodes a 26-kDa polypeptide of 231 amino acids. The product of *orfB* shares 78% amino acid similarity with the product of a *Staphylococcus aureus* gene that was identified as the insertion site for the transposon Tn*554* (27). The function of the *S. aureus* gene is unknown. This ORF is also 69% similar at the amino acid level to the *E. coli radC* gene product (37). Southern blotting experiments using chromosomal DNA from wild-type cells and from ϕ105 lysogens indicate that the ϕ105 attachment site is located between the *Sma*I and *Eco*RI sites in *orfB* (14a, 23, 23a). These results confirm mapping experiments that position the phage attachment site between *rodB1* and *spoIIB* on the *B. subtilis* chromosome (16).

Evidence presented below will show that the five remaining ORFs are part of a five-cistron operon. The first three ORFs in this operon have predicted sizes of 337 (36,159 Da), 290 (32,155 Da), and 173 (19,783 Da) codons and show various degrees of similarity to the *E. coli* shape-determining genes *mreB*, *mreC*, and *mreD*. Figures 4 and 5 show alignments of the *E. coli* and *B. subtilis mre* gene products. The product of the gene designated *mreB* in Fig. 1 shares 57.8% identity with *E. coli* MreB (Fig. 4) and an identity with the *B. cereus mreB* product that approaches 66% in certain stretches of the amino acid sequences (not shown). Although the *B. subtilis mreC*-like gene product does not exhibit high overall similarity to *E. coli* MreC, regions of significant similarity exist between the predicted product of the *mreC*-like gene and the corresponding *E. coli* protein (Fig. 5A). As a result of its position following *B. subtilis mreB* and *mreC* and its size, we presume that the product of the third gene of the operon, *mreD*, is the homolog to *E. coli* MreD, although it has only a 21% identity with the *E. coli* protein according to a Best-fit (12a) analysis (not shown).

The last two genes in the operon encode proteins with lengths of 227 (24,965 Da) and 269 (29,338 Da) amino acids. The product of the penultimate gene, *minC*, shares regions of similarity with the *E. coli* MinC protein (Fig. 5B). Likewise, the protein encoded by the last gene in the operon, designated *minD*, is 44.3% identical to the *E. coli minD* gene product. A Best-fit (12a) alignment of the predicted *B. subtilis* MinD and *E. coli* MinD is shown in Fig. 6. As noted in Fig. 2 of Cutting et al. (6), *B. subtilis minD* is followed by a region of dyad symmetry that may serve as a rho-independent terminator for the operon.

Localization of *rodB1* mutation. The *rodB1* mutation is a conditional mutation that causes the formation of rounded and irregularly shaped cells when mutant cells are grown under restrictive conditions (i.e., low salt concentration or temperatures above 42°C) (32). For an example of the *rodB1* phenotype, note the irregularly shaped cells in Fig. 2C. Because *rodB1* is located between the *spoIIB* and *divIVB* loci (20, 22) and because the *rodB1* mutant phenotype is strikingly similar to that of the *E. coli mre* (*envB*) mutants (39), we reasoned that *rodB1* might be allelic to one of the *B. subtilis mre* genes. In confirmation of this expectation, integration of pPL1 (Fig. 1) into the chromosome of a strain carrying the *rodB1* mutation corrected the *rod* phenotype of a *rodB1* mutant (Fig. 2D) and at the same time created a slight minicell phenotype, the basis for which will be discussed below. In contrast to these results, the integration of pSC224 into the *rodB1* strain did not correct the *rodB1* mutation. We conclude, then, that the *rodB1* mutation lies between the *Bgl*II site at the upstream boundary of the insert in pPL1 and the *Pst*I site at the upstream end of the insert in pSC224. Thus, the wild-type allele of *rodB1* is most likely located within the region of the three *B. subtilis mre* genes. Varley and Stewart (37a) have reported further localization of the *rodB1* allele to the *mreD* cistron.

Determining the boundaries of the operon. To define the functional boundaries of the transcriptional unit(s) encompassing *minC* and *minD*, we used plasmids containing DNA internal to the *min* genes and the *mre* genes as well as plasmids with inserts that overlapped the ends of the open reading frames of these genes. Since the integrational plasmids did not contain origins of replication for *B. subtilis*, transformants obtained by drug selection (Cm^r) for the vector-specific chloramphenicol resistance gene (*cat*) arise from single reciprocal (Campbell-like) recombination between the plasmid insert and the corresponding region of DNA in the chromosome (43, 44). Fragments internal to the operon will separate the chromosomal region homologous to

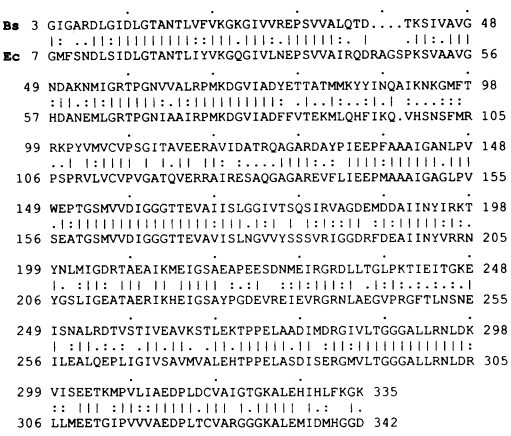

FIG. 4. Best-fit (12a) amino acid sequence alignment of the *E. coli* (Ec) and *B. subtilis* (Bs) *mreB* gene products. The *E. coli* MreB sequence is from Doi et al. (13). Lines denote identical amino acids, and dots denote amino acids which are conserved to a greater (:) or lesser (·) degree between the two sequences.

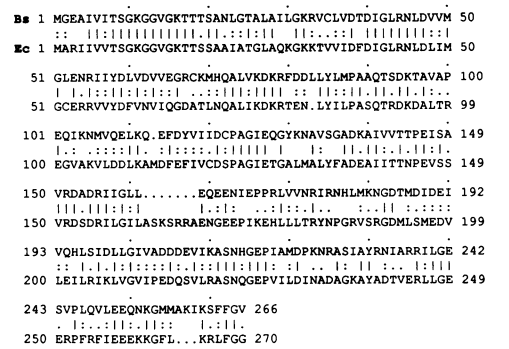

FIG. 6. Best-fit (12a) amino acid sequence alignment of the *E. coli* (Ec) and *B. subtilis* (Bs) *minD* gene products. The *E. coli* MinD sequence is from de Boer et al. (11). Lines denote identical amino acids, and dots denote amino acids which are conserved to a greater (:) or lesser (·) degree between the two sequences.

the plasmid insert from upstream promoters, thereby disrupting the operon in a polar manner.

As shown in Fig. 1, the integration of pPL6, which contains DNA internal to *minC* and *minD*, into the wild-type strain PY79 resulted in a minicell phenotype that was more severe than that exhibited by the classical *divIVB1* mutation. Similar to the results obtained with pPL6, the integration of plasmid pPL5, whose insert is internal to *mreB* and *mreC*, into PY79 results in a severe minicell phenotype (Fig. 1). This result indicates that *minC* and *minD* are part of the same transcriptional unit as the *mre* genes. Although disruption of the *B. subtilis mre* genes causes a minicell phenotype, it did not result in a *rod* phenotype, as is observed to occur when the *E. coli mreB*, *mreC*, or *mreD* genes are disrupted (38, 41). Possible explanations for this surprising result are discussed below.

In contrast to the results obtained with pPL1, pPL5, and pPL6, the integration of pPM57, whose insert overlaps the upstream end of *mreB*, or pSC224, whose insert overlaps the downstream end of *minD*, into the wild-type strain did not cause a minicell phenotype (Fig. 1). These results indicate that the *mre* genes and the *min* genes are part of the same transcriptional unit whose upstream boundary precedes *mreB* in the region corresponding to the insert in pPM57 and whose downstream boundary is between *minD* and *spoIVF* in the region corresponding to the insert in pPL1.

The integration into the chromosome of PY79 of plasmids pPL7 and pPM53, whose inserts extend from within *mreB* to an *Eco*RI site located 325 bp upstream of the *mreB* start codon, did not cause the severe minicell phenotype exhibited by integration of pPL5 and pPL6 (Fig. 1). Nevertheless, the transformants did exhibit a slight minicell phenotype. This is in contrast to the wild-type phenotype observed following integration of pPM56 and pPM54, whose inserts overlap *mreB* but extend more than 1 kb upstream of the *Eco*RI site (Fig. 1). A possible interpretation of these results is that transcription for the *mre* and *min* operon is generated from at least two promoters, one of which is downstream of the *Eco*RI site. We infer that the downstream promoter is inadequate to direct the synthesis of sufficient MinC and MinD to fully suppress the minicell phenotype.

Finally, we consider the case of pPL1, whose insert extends from within *mreB* to the stop codon at the end of *minD*. Integration of pPL1 into the chromosome of PY79 results in a slight minicell phenotype, similar to the partial minicell phenotype that had been observed following the integration of pPL1 into the chromosome of the *rodB1* and *divIVB1* strains (see above). From the examination of vector sequence and the sequence at the downstream boundary of its insert, we infer that integration of pPL1 was expected to eliminate the *minD* stop codon and thereby extend the *minD* ORF an additional 18 codons into vector DNA. Evidently, the resulting elongated MinD protein is only partially functional.

Determining transcript length via Northern hybridization. To confirm that *mreBCD* and *minCD* constitute a single operon, we carried out Northern hybridization with RNA from cells harvested at the end of and 2 h after the end of exponential growth in DS medium. The results show that both an *mre*-specific probe (pPL5) and a *min*-specific probe (pPL6) hybridized to a 4- to 5-kb RNA species, creating the smears shown in Fig. 7. The darker bands within the smear in Fig. 7A correspond to 16S and 23S rRNAs. The level of transcript decreased 2 h after the end of exponential growth (not shown). The smearing is most likely due to the degra-

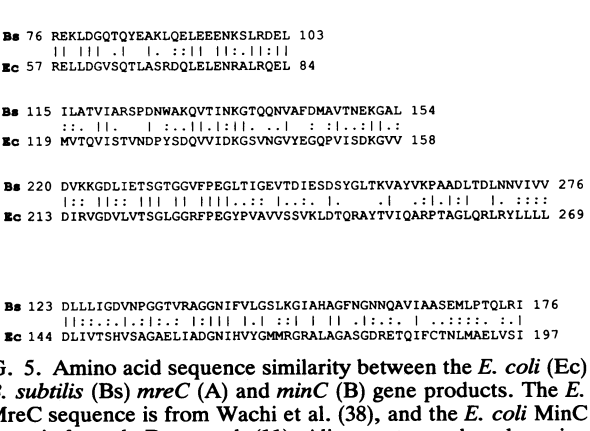

FIG. 5. Amino acid sequence similarity between the *E. coli* (Ec) and *B. subtilis* (Bs) *mreC* (A) and *minC* (B) gene products. The *E. coli* MreC sequence is from Wachi et al. (38), and the *E. coli* MinC sequence is from de Boer et al. (11). Alignment was done by using the Best-fit program. Lines denote identical amino acids, and dots denote amino acids which are conserved to a greater (:) or lesser (·) degree between the two sequences.

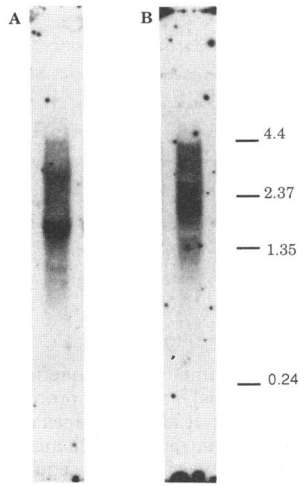

FIG. 7. (A) Northern blot analysis of 30 μg of *mreBC* RNA harvested just at the end of exponential growth ($t = 0$). The *mreBC* DNA fragment used was an 0.9-kb fragment from pPL5 (Fig. 1). (B) The same blot probed for *minCD* RNA. The *minCD* DNA is a 1.1-kb fragment from pPL6 (Fig. 1). Dark bands are 23S and 16S rRNA subunits. Smearing is most likely due to degradation of the mRNAs. Size markers along the edge of the gel are in kilobases.

dation of the mRNAs. (In a control experiment, hybridization to the same Northern blot of a segment of DNA internal to the *spoIIA* operon labeled a 1.7-kb RNA harvested 2 h after the end of exponential growth [not shown], a result consistent with the known size of the *spoIIA* transcript [36]). Since the combined length of the three *mre* genes and the two *min* genes is just under 4 kb, the length of the labeled transcript is adequate to include all five genes.

DISCUSSION

We have cloned and characterized DNA in the vicinity of the *divIVB* locus in *B. subtilis*, a chromosomal region flanked by the sporulation genes *spoIIB* and *spoIVF*. This region was found to contain seven ORFs, two of which are predicted to encode polypeptides with regions of significant amino acid similarity to the products of the *E. coli* cell division genes *minC* and *minD* (Fig. 1, 5B, and 6). The product of the putative *B. subtilis minC* gene is similar to *E. coli* MinC in a region that is thought to be responsible for interactions with the *E. coli* cell division proteins MinD and DicB (26). In agreement with the view that the *B. subtilis minC*- and *minD*-like genes are involved with septum placement, this DNA is the site of the *divIVB1* minicell mutation (Fig. 2A). Unlike the *minB* operon of *E. coli*, which consists of *minC*, *minD*, and *minE* genes, no homolog of *E. coli minE* is found at the *divIVB* locus, as the next gene downstream of *minC* and *minD* is the first member of the sporulation operon *spoIVF*.

The *B. subtilis minC* and *minD* genes are preceded by three additional ORFs, which, as demonstrated by disruptional integration (Fig. 1) and Northern hybridization experiments (Fig. 7), are part of the same transcriptional unit. The predicted products of these three genes are similar to a greater or lesser extent to the products of the *E. coli* shape-determining genes *mreB*, *mreC*, and *mreD* (Fig. 1, 4, and 5A). In agreement with the view that the *B. subtilis* ORFs play a role in shape determination, this DNA was found to be the site of *rodB1*, a mutation that causes the formation of rounded and irregularly shaped cells under restrictive conditions. In confirmation and extension of these results, Varley and Stewart have further localized *rodB1* to the *mreD* cistron (37a). Thus, unlike the case in *E. coli*, shape-determining and minicell genes in *B. subtilis* are part of the same transcriptional unit.

While disruption of the *divIVB* operon with integrational plasmids causes a mild to severe minicell phenotype in transformed cells, it does not cause a *rod* phenotype. This is an unexpected result, as null mutations in any of the three *E. coli mre* genes result in a *rod* phenotype (39, 41). A possible explanation for the lack of apparent phenotype following disruption of *mreC* and *mreD* may lie in the existence of a second copy of the *mre* genes at a separate locus. In fact, a second ORF with significant homology to *E. coli mreB* as well as to the *B. subtilis mreB* isolated in this study has been found at a position downstream of the sporulation locus *spoIIID* (5). It is not yet known whether this second copy of *mreB* is part of an operon that also encodes copies of *mreC* and *mreD*. If it is the case that a second *mre* locus exists, our results imply that the original *rodB1* mutation was a gain-of-function mutant. An alternative explanation for the lack of phenotype following disruption of the *mre* genes may be the existence of a cryptic promoter in the integrational vector pSGMU2 that is strong enough to drive sufficient transcription of *mreC* and *mreD* to prevent a *rod* phenotype but is not strong enough to transcribe *minC* and *minD* sufficiently to overcome the minicell phenotype. To determine which of the two explanations is correct, it will be necessary to construct true null mutations of each of the *mre* genes.

Although disruption of the *divIVB* operon resulted in a minicell phenotype, the sporulation efficiencies of these disruptional mutants as well as that of the classical *divIVB1* mutant were similar to that of PY79, the wild-type strain (22a). This result is not unexpected, given that the role of the *E. coli minC* and *minD* gene products is to block both the polar and nonpolar division sites and that it is the third gene in the *minB* operon, *minE*, which conveys topological specificity. If the *B. subtilis min* homologs are involved in sporulation, *B. subtilis minCD* mutants might be expected to form asymmetric septa two out of three times and would thus have an expected sporulation efficiency of 66%, a deviation from wild-type efficiency which we would not be able to measure in a meaningful manner by using the assay for heat-resistant spores. Such a result would be consistent with the fact that *min* mutations appear to have little effect on the growth rate of vegetative cells, although they septate correctly only one out of three times.

During cell division in *E. coli*, the *minE* gene product functions to prevent the MinCD complex from inactivating the central site while allowing it to block septation at polar sites (11). We speculate that a homolog or pair of homologs to *E. coli minE*, the *min* gene that was not found at the *divIVB* locus, is responsible for determining the topological specificity of the *B. subtilis minC* and *minD* gene products. In one model, a single MinE homolog inactivates the MinCD complex at midcell during vegetative growth in a manner similar to that of *E. coli* MinE. During sporulation, this MinE homolog undergoes some kind of modification that causes it to inactivate the MinCD complex at polar sites and not at midcell, thereby allowing the formation of an asymmetrically positioned septum. In an alternative model, *B. subtilis* possesses two *minE*-like genes, one expressed during growth and one expressed early during sporulation. The vegetatively expressed *minE* would allow the formation of medial

septa, whereas the sporulation-specific gene would cause the appearance of asymmetrically positioned septa.

In summary, we report here the cloning of a five-cistron operon in *B. subtilis* whose predicted proteins are similar to the products of the *E. coli* shape-determining genes *mreB*, *mreC*, and *mreD* and the *E. coli* cell division genes *minC* and *minD*. The *mre* genes are the site of the cell shape-altering mutation *rodB1*, whereas the *min* genes are the site of the minicell mutation *divIVB1*. A homolog or homologs of the *E. coli minE* gene, which was absent from the *divIVB* operon, could govern the position of septum placement during growth and sporulation.

ACKNOWLEDGMENTS

We are grateful to George Stewart for communicating his results prior to publication. Don Dubin performed part of the sequencing that defined the ORF at the Tn*554* insertion site in *S. aureus*. We also thank Steve Roels for his assistance with computer analysis of sequencing data and Patrick Stragier for assistance with the mapping of the ϕ105 attachment site.

This work was supported by grants GM18568 and GM19698 from NIH to R.L. and P.S. and by a predoctoral fellowship from the National Science Foundation to P.S.M.

REFERENCES

1. **Adler, H. I., W. D. Fisher, A. Cohen, and A. H. Hardigree.** 1967. Miniature *Escherichia coli* cells deficient in DNA. Proc. Natl. Acad. Sci. USA **57**:321–326.
2. **Beall, B., and J. Lutkenhaus.** 1991. FtsZ in *Bacillus subtilis* is required for vegetative septation and for asymmetric septation during sporulation. Genes Dev. **5**:447–455.
3. **Beall, B., and J. Lutkenhaus.** 1992. Impaired cell division and sporulation of a *Bacillus subtilis* strain with the *ftsA* gene deleted. J. Bacteriol. **174**:2398–2403.
4. **Bi, E., and J. Lutkenhaus.** 1990. Interaction between the *min* locus and *ftsZ*. J. Bacteriol. **172**:5610–5616.
5. **Bosma, A., and R. Losick.** 1992. Personal communication.
6. **Cutting, S., S. Roels, and R. Losick.** 1991. Sporulation operon *spoIVF* and the characterization of mutations that uncouple mother-cell from forespore gene expression in *Bacillus subtilis*. J. Mol. Biol. **221**:1237–1256.
7. **Cutting, S. M., and P. B. Vander Horn.** 1990. Genetic analysis, p. 27–74. *In* C. R. Harwood, and S. M. Cutting (ed.), Molecular biological methods for *Bacillus*. John Wiley and Sons, Chichester, England.
8. **Davie, E., K. Snydor, and L. I. Rothfield.** 1984. Genetic basis of minicell formation in *Escherichia coli* K-12. J. Bacteriol. **158**: 1202–1203.
9. **de Boer, P. A. J., W. R. Cook, and L. I. Rothfield.** 1990. Bacterial cell division. Annu. Rev. Genet. **24**:249–274.
10. **de Boer, P. A. J., R. E. Crossley, and L. I. Rothfield.** 1988. Isolation and properties of *minB*, a complex genetic locus involved in correct placement of the division site in *Escherichia coli*. J. Bacteriol. **170**:2106–2112.
11. **de Boer, P. A. J., R. E. Crossley, and L. I. Rothfield.** 1989. A division inhibitor and a topological specificity factor coded for by the minicell locus determine proper placement of the division septum. Cell **56**:641–649.
12. **de Boer, P. A. J., R. E. Crossley, and L. I. Rothfield.** 1990. Central role for the *Escherichia coli minC* gene product in two different cell division-inhibition systems. Proc. Natl. Acad. Sci. USA **87**:1129–1133.

12a. **Devereux, J., P. Haeberli, and O. Smithies.** 1984. A comprehensive set of sequence analysis programs for the VAX. Nucleic Acids Res. **12**:387–395.

13. **Doi, M., M. Wachi, F. Ishino, S. Tomioka, M. Ito, Y. Sakagami, A. Suzuki, and M. Matsuhashi.** 1988. Determinations of the DNA sequence of the *mreB* gene and of the gene products of the *mre* region that function in formation of the rod shape of *Escherichia coli* cells. J. Bacteriol. **170**:4619–4624.
14. **Dubnau, D., and R. Davidoff-Abelson.** 1971. Fate of transforming DNA following uptake by competent *Bacillus subtilis*. J. Mol. Biol. **56**:209–221.

14a. **Ellis, E., and D. H. Dean.** 1986. Location of the *Bacillus subtilis* temperate phage ϕ105 *attP* attachment site. J. Virol. **58**:223–224.

15. **Fort, P., and J. Errington.** 1985. Nucleotide sequence and complementation analysis of a polycistronic sporulation operon, *spoVA*, in *Bacillus subtilis*. J. Gen. Microbiol. **131**:1091–1105.
16. **Henner, D. J., and J. A. Hoch.** 1980. The *Bacillus subtilis* chromosome. Microbiol. Rev. **44**:57–82.
17. **Hitchins, A. D., and R. A. Slepecky.** 1969. Bacterial sporulation as a modified procaryotic cell division. Nature (London) **233**: 804–807.
18. **Hoch, J. A.** 1971. Genetic analysis of pleiotropic negative sporulation mutants in *Bacillus subtilis*. J. Bacteriol. **105**:896–901.
19. **Jaffe, A., E. Boye, and R. D'Ari.** 1990. Rule governing the division pattern in *Escherichia coli minB* and wild-type filaments. J. Bacteriol. **172**:3500–3502.
20. **Karamata, D., M. McConnell, and H. J. Rogers.** 1972. Mapping of *rod* mutants of *Bacillus subtilis*. J. Bacteriol. **111**:73–79.
21. **Labie, C., F. Bouche, and J.-P. Bouche.** 1990. Minicell-forming mutants of *Escherichia coli*: suppression of both DicB- and MinD-dependent division inhibition by inactivation of the *minC* gene product. J. Bacteriol. **172**:5852–5855.
22. **Lamont, I. L., and J. Mandelstam.** 1984. Identification of a new sporulation locus, *spoIIIF*, in *Bacillus subtilis*. J. Gen. Microbiol. **130**:1253–1261.

22a. **Levin, P. A.** Unpublished data.

23. **Margolis, P. S.** Unpublished data.

23a. **Marrero, R., and R. E. Yasbin.** 1986. Evidence for circular permutation of the prophage genome of *Bacillus subtilis* bacteriophage ϕ105. J. Virol. **57**:1145–1148.

24. **Miyakawa, Y., and T. Komano.** 1981. Study on the cell cycle of *Bacillus subtilis* using temperature-sensitive mutants. I. Isolation and genetic analysis of the mutants defective in septum formation. Mol. Gen. Genet. **181**:207–214.
25. **Moran, C. P., Jr., N. Lang, S. F. J. Legrice, G. Lee, M. Stephens, A. L. Sonenshein, J. Pero, and R. Losick.** 1982. Nucleotide sequences that signal the initiation of transcription and translation in *Bacillus subtilis*. Mol. Gen. Genet. **186**:339–346.
26. **Mulder, E., C. L. Woldringh, F. Tétart, and J.-P. Bouché.** 1992. New *minC* mutations suggest different interactions of the same region of division inhibitor MinC with proteins specific for *minD* and *dicB* coinhibition pathways. J. Bacteriol. **174**:35–39.
27. **Murphy, E. (The Public Health Research Institute of the City of New York, Inc.).** 1992. Personal communication.
28. **Nicholson, W. L., and P. Setlow.** 1990. Sporulation, germination and outgrowth, p. 391–450. *In* C. R. Harwood, and S. M. Cutting (ed.), Molecular biological methods for *Bacillus*. John Wiley and Sons, Chichester, England.
29. **Reeve, J. N., N. H. Mendelson, L. I. Coyne, L. L. Hallock, and R. M. Cole.** 1973. Minicells of *Bacillus subtilis*. J. Bacteriol. **114**:860–873.
30. **Roels, S., A. Driks, and R. Losick.** 1992. Characterization of *spoIVA*, a sporulation gene involved in coat morphogenesis in *Bacillus subtilis*. J. Bacteriol. **174**:575–585.
31. **Roels, S., and R. Losick.** 1991. Personal communication.
32. **Rogers, H. J., M. McConnell, and I. D. J. Burdett.** 1970. The isolation and characterization of mutants of *Bacillus subtilis* and *Bacillus licheniformis* with disturbed morphology and cell division. J. Gen. Microbiol. **61**:155–171.
33. **Sambrook, J., E. F. Fritsch, and T. Maniatis.** 1989. Molecular cloning: a laboratory manual, 2nd ed. Cold Spring Harbor Laboratory, Cold Spring Harbor, N.Y.
34. **Sandman, K., R. Losick, and P. Youngman.** 1987. Genetic analysis of *Bacillus subtilis spo* mutations generated by Tn*917*-mediated insertional mutagenesis. Genetics **117**:603–617.
35. **Sanger, F., S. Nicklen, and A. R. Coulson.** 1977. DNA sequencing with chain-terminating inhibitors. Proc. Natl. Acad. Sci. USA **74**:5463–5467.
36. **Savva, D., and J. Mandelstam.** 1986. Synthesis of *spoIIA* and

spoVA mRNA in *Bacillus subtilis*. J. Gen. Microbiol. **132**:3005–3011.

37. **Stewart, G. C. (The University of South Carolina).** 1992. Personal communication.

37a. **Varley, A. W., and G. C. Stewart.** 1992. The *divIVB* region of the *Bacillus subtilis* chromosome encodes homologs of *Escherichia coli* septum placement (MinCD) and cell shape (MreBCD) determinants. J. Bacteriol. **174**:6729–6742.

38. **Wachi, M., M. Doi, Y. Okada, and M. Matsuhashi.** 1989. New *mre* genes *mreC* and *mreD*, responsible for formation of the rod shape of *Escherichia coli* cells. J. Bacteriol. **171**:6511–6516.

39. **Wachi, M., M. Doi, S. Tamaki, W. Park, S. Nakajima-Iijima, and M. Matsuhashi.** 1987. Mutant isolation and molecular cloning of *mre* genes, which determine cell shape, sensitivity to mecillinam, and amount of penicillin-binding proteins in *Escherichia coli*. J. Bacteriol. **169**:4935–4940.

40. **Wachi, M., M. Doi, R. Ueda, M. Ueki, K. Tsuritani, K. Nagai, and M. Matsuhashi.** 1991. Sequence of the downstream flanking region of the shape-determining genes *mreBCD* of *Escherichia coli*. Gene **106**:135–136.

41. **Wachi, M., and M. Matsuhashi.** 1989. Negative control of cell division by *mreB*, a gene that functions in determining the rod shape of *Escherichia coli* cells. J. Bacteriol. **171**:3123–3127.

42. **Youngman, P.** 1990. Use of transposons and integrational vectors for mutagenesis and construction of gene fusions in *Bacillus* species, p. 221–266. *In* C. R. Harwood, and S. M. Cutting (ed.), Molecular biological methods for *Bacillus*. John Wiley and Sons, Chichester, England.

43. **Youngman, P., J. B. Perkins, and K. Sandman.** 1984. New genetic methods, molecular cloning strategies, and gene fusion techniques for *Bacillus subtilis* which take advantage of Tn917 insertional mutagenesis, p. 103–111. *In* J. A. Hoch and A. T. Ganesan (ed.), Genetics and biotechnology of bacilli. Academic Press, Inc., New York.

44. **Youngman, P. J., J. B. Perkins, and R. Losick.** 1984. A novel method for rapid cloning in *Escherichia coli* of *Bacillus subtilis* chromosomal DNA adjacent to Tn*917* insertions. Mol. Gen. Genet. **195**:424–433.